Influence of growth temperature on the pinning landscape of $YBa_2Cu_3O_{7-\delta}$ films grown from Ba-deficient solutions

OPEN ACCESS
IOP Publishing
Superconductor Science and Technology
Supercond. Sci. Technol. **35** (2022) 104004 (8pp)
https://doi.org/10.1088/1361-6668/ac8580

Influence of growth temperature on the pinning landscape of $YBa_2Cu_3O_{7-\delta}$ films grown from Ba-deficient solutions

Jordi Alcalà[1], Pau Ternero[1], Cornelia Pop[1], Laura Piperno[2], Susagna Ricart[1], Narcís Mestres[1], Teresa Puig[1], Xavier Obradors[1], Alexander Meledin[3,4], Giuseppe Celentano[2] and Anna Palau[1,*]

[1] Institut de Ciència de Materials de Barcelona, ICMAB-CSIC, Campus UAB, 08193 Bellaterra, Spain
[2] ENEA, Frascati Research Centre, Via E. Fermi, 45-00044, Frascati, Italy
[3] Ernst Ruska Centre for Microscopy and Spectroscopy with Electrons, Jülich Research Center, Wilhelm-Johnen-Straße, 52425 Jülich, Germany

E-mail: palau@icmab.es

Received 27 April 2022, revised 26 July 2022
Accepted for publication 29 July 2022
Published 6 September 2022

Abstract

Cuprate coated conductors are promising materials for the development of large-scale applications, having superior performance over other superconductors. Tailoring their vortex pinning landscape through nanostructure engineering is one of the major challenges to fulfill the specific application requirements. In this work, we have studied the influence of the growth temperature on the generation of intrinsic pinning defects in $YBa_2Cu_3O_{7-\delta}$ films grown by chemical solution deposition using low Ba precursor solutions. We have analysed the critical current density as a function of the temperature, applied magnetic field magnitude and orientation, $J_c(T,H,\theta)$, to elucidate the nature and strength of pinning sites and correlate the microstructure of the films with their superconducting performance. An efficient pinning landscape consisting of stacking faults and associated nanostrain is naturally induced by simply tuning the growth temperature without the need to add artificial pinning sites. Samples grown at an optimized temperature of 750 °C show very high self-field J_c values correlated with an overdoped state and improved $J_c(T,H,\theta)$ performances.

Keywords: high-temperature superconductors, critical current density, vortex pinning, chemical solution deposition

(Some figures may appear in colour only in the online journal)

[4] Current address: Thermo Fisher Scientific, Achtseweg Noord 5, 5651 GG Eindhoven, The Netherlands.
[*] Author to whom any correspondence should be addressed.

1. Introduction

Superconducting cuprate $YBa_2Cu_3O_{7-\delta}$ (YBCO), or other rare earth equivalents $REBa_2Cu_3O_{7-d}$ (REBCO) coated conductors hold great promise to revolutionize electrical power, generation, distribution and use, which could become more efficient and reliable, facing global challenges related to sustainable energy. In particular, REBCO materials offer a realistic vision for emerging energy and power applications to be operated at different temperature-magnetic field conditions, such as fusion reactors, electric motors, generators or highly efficient power grids [1, 2]

In this framework, many different strategies are adopted for the fabrication of nanocomposites (YBCO films with non-superconducting secondary faces) to induce artificial pinning centres with controlled dimensionality, density and size, able to pin vortices at the desired magnetic field/temperature conditions, using different growth methodologies. Moreover, simple and cost-effective processes able to be scaled for superconducting tape fabrication are strongly required [3, 4].

Chemical solution deposition (CSD) using low-fluorine trifluoroacetate (TFA) precursor solutions appears as a very promising process to fabricate REBCO coated conductors, since high performances can be obtained by a simple non-vacuum low-cost technique using environmentally friendly solutions [5–7].

Among the different parameters that may be changed to optimize the performance of CSD films, one can play with the stoichiometry of the starting solution. In this sense, Ba-deficient compositions have shown improved performances with extremely high critical current density values [8–10]. In a recent publication, we observed that by using low-fluorine Ba-deficient solutions, YBCO *c*-axis nucleation can be obtained at much lower temperatures ($T \sim 730$ °C) than those needed in stoichiometric films, thus significantly extending the epitaxial temperature growth window [8]. The growth temperature plays an important role on the amount and nature of the pinning defects induced within the YBCO matrix, and the associated pinning anisotropy and strength [11, 12]. So, growth temperature can be used to naturally tune the defect pinning landscape of YBCO films without the need to incorporate additional secondary phases. We demonstrated in [8] that by using an optimal growth temperature of 750 °C, which gave a good compromise between percolation (good texture) and pinning performance, we can obtain very high self-field critical current values, 60 MA cm^{-2} and 7 MA cm^{-2}, at 5 K and 77 K, respectively. Moreover, we observed that samples grown at lower temperatures showed smoother $J_c(H)$ dependencies evidencing a higher density of defects in the YBCO matrix. In this contribution, we have carefully analysed the morphology, angular, field and temperature dependence of the critical current of these samples as compared to pristine and nanocomposite YBCO films, in order to elucidate the nature and strength of pinning centres naturally induced when growing at low temperatures. The influence of the precursor solution and growth temperature on the doping level of the films has also been evaluated.

2. Methodology

Low-fluorine Ba-deficient precursor solutions were prepared by dissolving barium, copper acetates, and yttrium TFA with a ratio of Y:Ba:Cu equal to 1:1.5:3 in a mixture of organic solvents consisting of propionic acid (30%) and methanol while heating at 30 °C [8]. Precursor solution was deposited by spin coating with an angular velocity of 6000 rpm, angular acceleration of 6000 rpm s^{-1} and spinning duration time of 2 min on 5 × 5 mm^2 (100) $LaAlO_3$ single-crystal substrates. The coatings were pyrolyzed up to 310 °C in a humid O_2 atmosphere and crystallized with heating ramp of 25 °C min^{-1} up to the desired growth temperature (810 °C and 750 °C) during 3 h. Afterwards we performed an oxygenation process at 500 °C. For comparison purposes, a stoichiometric pristine YBCO film and a nanocomposite (12% $BaHfO_3$ (BHO) nanoparticles) were grown at 810 °C following the same process, but by using a standard stoichiometric (Y:Ba:Cu-1:2:3) TFA solution with yttrium, barium and copper TFA [13]. The thickness of all films analysed was $t \sim 200$ nm.

The structural quality of the samples was determined by x-ray diffraction (XRD) using a 2D Bruker AXS general area detector diffraction system operating with Cu K_α and scanning electron microscopy (SEM) using an FEI Quanta 200 FEG system. Transport measurements were performed using a four-probe configuration in patterned tracks of 30 μm of width and 250 μm length, using a Quantum Design physical property measurement system (PPMS). Angular curves of the critical current density, $J_c(\theta)$, were obtained at temperatures ranging from $T = 5$–77 K and magnetic fields from $\mu_0 H = 0$–9 T, considering the orientations $\theta = 90°$ for $H//ab$ and $\theta = 180°$ for $H//c$. The critical current was determined with an electric field criterion of 2 μV cm^{-1}. Hall effect measurements were carried out also by the PPMS at 300 K using the Van der Pauw configuration [14] in the field range of −9 T to 9 T. The charge carrier density, n_H, was calculated at 300 K as $n_H = 1/(qR_H)$; where q is the charge of the electron and R_H the Hall coefficient [15]. High-angle annular dark-field (HAADF) scanning transmission electron microscopy (STEM) imaging was carried out on an FEI Titan ChemiSTEM probe Cs-corrected transition electron microscopy (TEM) operated at 200 kV [16].

3. Results and discussion

We compare four YBCO films; two stoichiometric YBCO samples (a pristine standard film (Stoich-810) and a nanocomposite (Stoich-NC-810) both grown at 810 °C), and two Ba-deficient samples (a film grown at 810 °C (LowBa-810), and another one grown at the optimized temperature of 750 °C (LowBa-750)).

Figure 1 shows the critical current density as a function of the magnetic field $H//c$ for these four samples at 77 K, in a log-log scale. The first thing that one can observe is that the $J_c(H)$ curves obtained for pristine stoichiometric and the Ba-deficient sample grown at 810 °C are almost identical, indicative of a minor effect of the precursor solution used. It

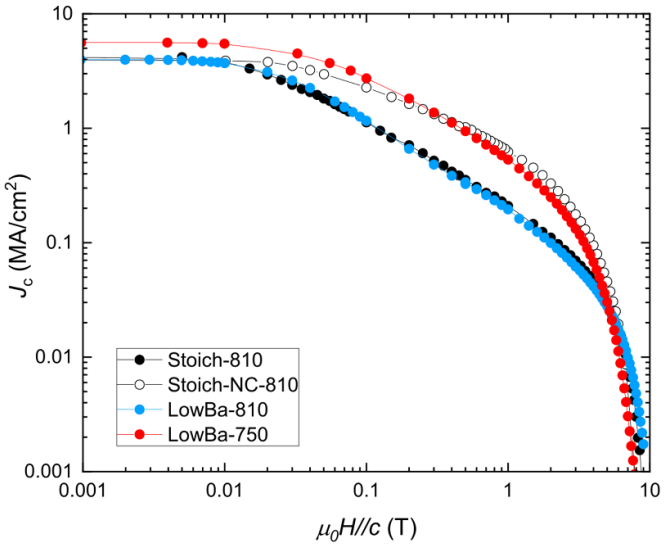

Figure 1. Critical current density values as a function of the applied magnetic field *H//c* at 77 K for samples: Stoich-810 (closed black dots), Stoich-NC-810 (opened black dots), LowBa-810 (closed blue dots) and LowBa-750 (closed red dots).

should be noted however that the growth temperature has a strong effect on the pinning performance. LowBa-750 shows a smother $J_c(H)$ dependence, similar to what we obtain in the nanocomposite film grown at 810 °C by introducing artificial pinning centres (BHO nanoparticles). We observe that efficient pinning sites can be naturally induced within the YBCO matrix by reducing the growth temperature, without the need to artificially introduce secondary phases. It should be noted that although both Stoich-NC-810 and LowBa-750 samples show a similar performance, there is a crossover of the $J_c(H)$ curves at ∼0.3 T. LowBa-750 shows a better self-field critical current density but a slightly faster J_c decay with the magnetic field, indicating that different defects are induced in the two samples.

A comprehensive discussion of artificially engineered pinning sites induced in YBCO nanocomposites with different nature and amount of nanoparticles (BHO, $BaZrO_3$, Ba_2YTaO_6 and Y_2O_3) can be found in [17]. In this work we aim to analyse the superconducting performance and associated pinning landscape in pristine Ba-deficient YBCO films grown at low temperature. We use a stoichiometric pristine and a typical nanocomposite film grown at 810 °C for comparison purposes.

Figure 2(a) shows a SEM image obtained for LowBa-750 were a uniform and flat surface with no *a*–*b* needle-shape grains are observed. XRD θ–2θ scan shown in figure 2(b) indicate a good epitaxial growth with *c*-axis YBCO (00 l) peaks. It should be noted that a small contribution of $Y_2Cu_2O_5$ reflections can be identified, consistent with the barium deficiency imposed by the Ba-deficient solution.

Figure 3 show the angular dependence of $J_c(\theta)$ obtained at 77 K–1 T, 65 K–5 T and 5 K–9 T for Stoich-810, Stoich-NC-810 and LowBa-750. By comparing the nanocomposite and the pristine sample grown at 810 °C (black open and closed symbols, respectively) we observe that effect of adding

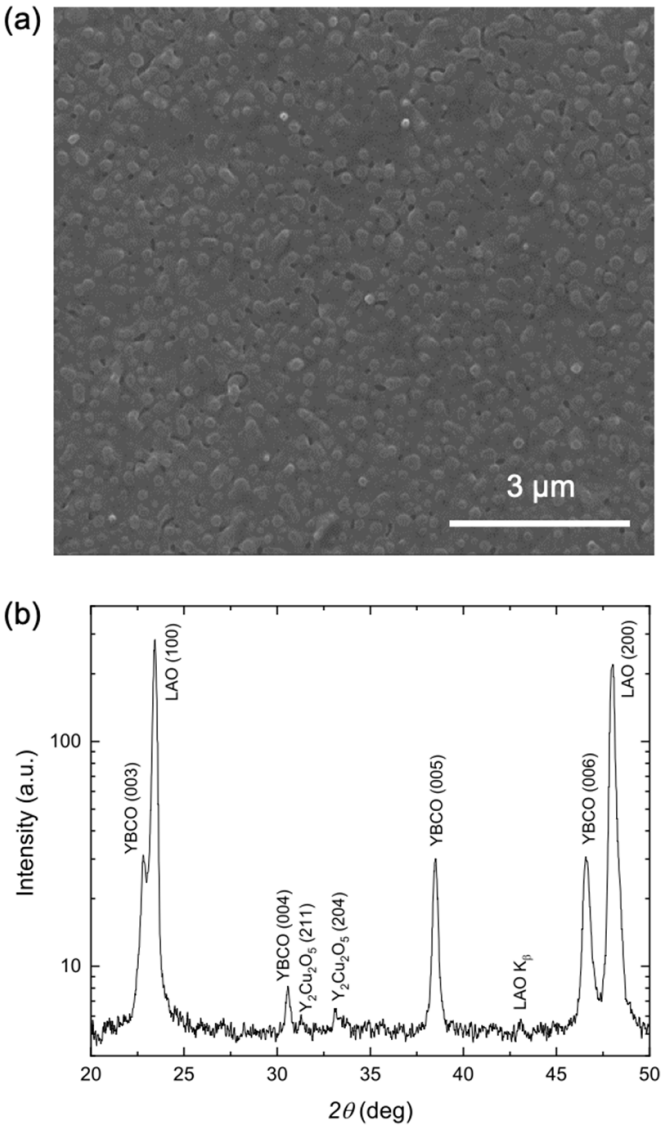

Figure 2. (a) SEM image and (b) XRD θ–2θ scan obtained for LowBa-810.

nanoparticles results in a broader *ab*-peak ($\theta = 90°$), attributed to the anisotropic pinning of stacking faults and higher values of J_c in the whole θ range, with a reduction of the anisotropy associated with the isotropic pinning of nanostrained regions induced at the partial dislocations at different fields and temperatures [18–20]. The $J_c(\theta)$ curves obtained for the pristine Ba-deficient sample grown at 750 °C (red symbols) show similar characteristics than that of the nanocomposite but with even much broader *ab*-peaks.

In general, in YBCO films the anisotropic pinning at *H//ab* mainly comes from the interplay between intrinsic pinning and stacking faults. The width of the $J_c(\theta)$ *ab*-peak can be associated to the trapping angle θ_T that limits the staircase regime where vortices accommodate to the anisotropic defects with kinks and parallel segments [21, 22]. Beyond θ_T vortices will be straight and take the direction of the applied field, thus being unaffected by the correlated nature of the anisotropic pinning.

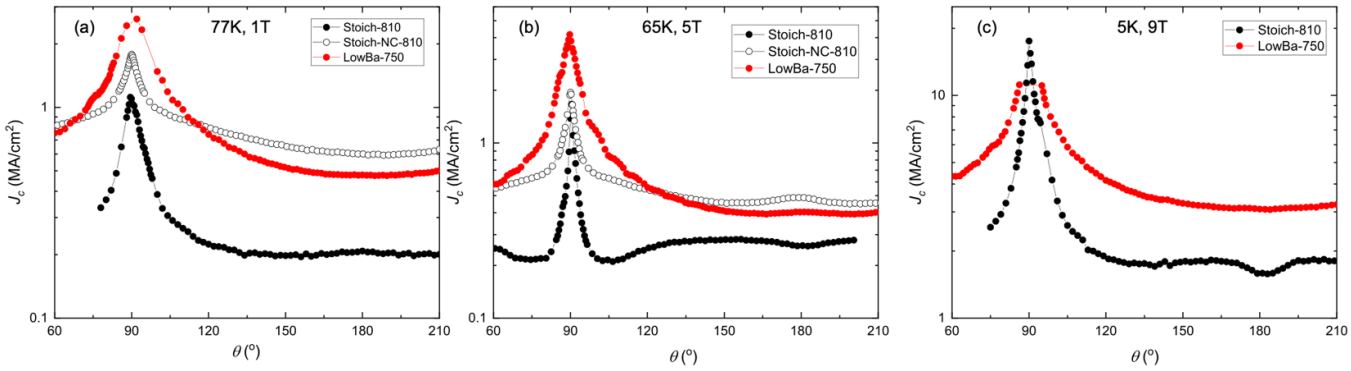

Figure 3. Angular dependence of the critical current density for samples Stoich-810 (closed black dots), Stoich-NC-810 (open black dots) and LowBa-750 (closed red diamonds) at (a) 77 K–1 T (b) 65 K-5 T and (c) 5 K–9 T.

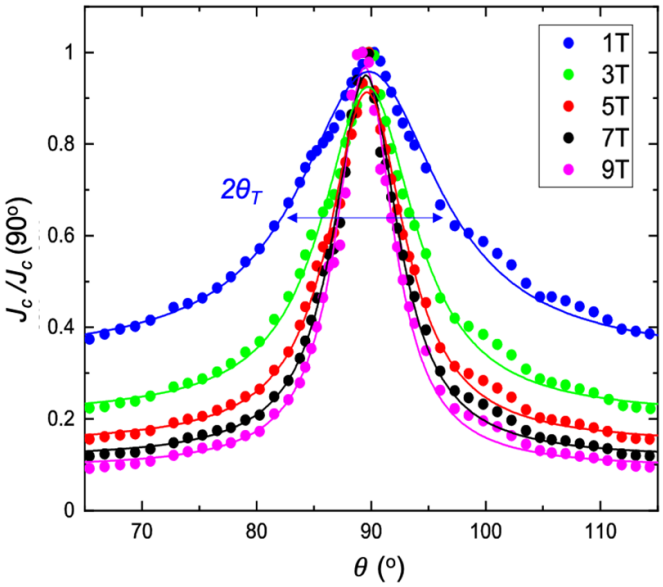

Figure 4. Angular dependence of the normalized critical current density at 90° and 65 K for different magnetic fields of the LowBa-750 sample. Solid lines are Lorentzian fits with $2\theta_T$ full with half maximum.

Figure 4 shows the normalized *ab*-peak measured at different magnetic fields for the LowBa-750 sample. Note that the width of the peak decreases as the field increases tending to a saturation at high fields. Field dependence of the trapping angle obtained for Stoich-810, Stoich-NC-810 and LowBa-750 at 77 K and 25 K is shown in figure 5. For both temperatures, the values of the trapping angle obtained for Stoich-NC-810 and LowBa-750 samples are much higher than those for Stoich-810, indicating that one can promote the formation of stacking faults either by introducing nanoparticles in a nanocomposite film or by reducing the growth temperature in a pristine film. It is worth noting that at low temperatures (figure 5(b)) the pristine stoichiometric sample grown at 810 °C (Stoich-810) shows a fast θ_T decrease with H and becomes constant above ∼4 T. Field independent θ_T can be associated with a single vortex pinning regime mainly dominated by intrinsic pinning with a very large matching field [21]. Samples with a high number of staking faults (Stoich-NC-810 and LowBa-750) do not reach the θ_T saturated region fingerprint of an extension of the pinning region dominated by stacking faults.

Figure 6 shows cross-section HAADF STEM images obtained for LowBa-750 at different magnifications, where we clearly observe the presence of a huge density of stacking faults as compared with a stoichiometric pristine film, were for a 200 × 200 N m^2 cross-section image less than 20 stacking faults are found [18].

To better elucidate the nature and strength of pinning sites induced in the Ba-deficient pristine YBCO film grown at 750 °C we analyse the contribution of different type of defects at different regions of the H–T phase diagram. A first classification of pinning centres may be performed considering their temperature dependence of the critical current density, $J_c(T)$. Weak pinning decay as an exponential function of T (equation (1)) [23] whereas strong pinning follows an exponential function of T^2 (equation (2)) [24]

$$J_c^{\text{weak}}(T) = J_c^{\text{weak}}(0)\ \exp\left(-\frac{T}{T_0}\right) \tag{1}$$

$$J_c^{\text{strong}}(T) = J_c^{\text{strong}}(0)\ \exp\left[-3\left(\frac{T}{T^*}\right)^2\right] \tag{2}$$

were $J_c^{\text{weak}}(0)$ and $J_c^{\text{strong}}(0)$ are the contributions to J_c at 0 K and T_0 and T^* the characteristic pinning energies of weak and strong pinning defects, respectively.

Another classification may be performed considering their shape. Isotropic pinning sites, with a pinning length that do not depend on the magnetic field orientation, and anisotropic pinning sites which are correlated along a certain field direction. These two kind of defects may be identified by using the Blatter scaling approach on a series of $J_c(\theta,H)$ curves plotted as a function of the effective magnetic field, H_{eff} (equation (3)) [25]

$$H^{\text{eff}} \sim H\left[\cos^2\theta + \gamma^{-1}\sin^2\theta\right]^{1/2} \tag{3}$$

were θ is the angle between the magnetic field and the c-axis and γ the anisotropy parameter.

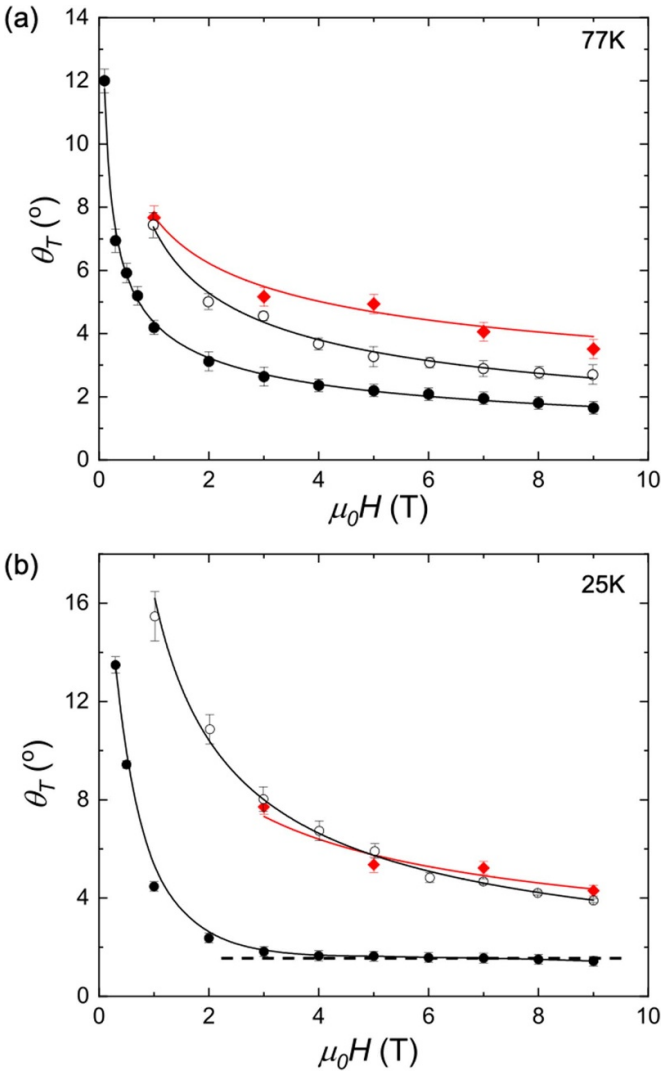

Figure 5. Magnetic field dependence of the trapping angle (θ_T) of different samples: Stoich-810 (closed black dots), Stoich-NC-810 (open black dots), LowBa-750 (closed red diamonds) at (a) 77 K and (b) 25 K. Dashed line is a guide to the eye to highlight the field independent θ_T region.

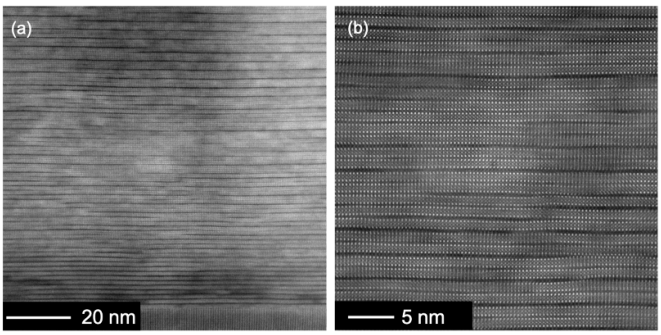

Figure 6. HAADF-STEM cross sections obtained for LowBa-750 at different magnifications. The dark horizontal stripes in the images correspond to stacking faults (Y124 intergrowths).

By combining equations (1)–(3) and adjusting angular, field and temperature dependence of $J_c(H,T,\theta)$, assuming a direct summation of pinning centres, one can determine and quantify three different pinning contributions: isotropic-weak (I-W), isotropic-strong (I-S), and anisotropic-strong (A-S) [26].

Figures 7 (a)–(c) plot log J_c versus T^2 at $\mu_0 H//c = 1$ T, $\mu_0 H//c = 9$ T and $\mu_0 H//ab = 9$ T. Linear fits to these plots correspond to strong pinning centres (equation (2)) which control J_c in the intermediate temperature regime. At low temperatures for $H//c$ the J_c values of Stoich-810 and Stoich-NC-810 deviate from the linear fit below ∼30 K at 1 T and 20 K at 9 T pointing out a region dominated by weak pinning defects [18]. In the case of LowBa-750 the linear dependence is observed down to lower temperatures, indicating that strong pinning centres control the pinning performance in a wider temperature region: 5 K–60 K at 1 T and 15 K–55 K at 9 T. At this low-intermediate temperature regime this sample shows the best J_c performance. At high temperatures, a fast decay of J_c is obtained in all the samples due to thermal fluctuations close to T_c. As pointed out above a crossover of the $J_c(T)$ curves of Stoich-NC-810 and LowBa-750 is obtained at 68 K–1 T and 65 K–9 T $H//c$ which may be associated to a slightly higher irreversibility line of the former [18].

In figures 7(d)–(f) we show the weights of the three basic pinning contributions of $J_c(T)$ for LowBa-750. At intermediate fields, $\mu_0 H//c = 1$ T, the most important contribution comes from I-S pinning which can be associated to nanostrain induced to accommodate the stacking faults [20]. At higher fields, $\mu_0 H//c = 9$ T, we observe that an important contribution of I-W defects appears at low temperature. These defects may be associated to Cu–O cluster vacancies appearing at the intergrowths [27]. At $\mu_0 H//ab = 9$ T the A-S contribution coming from stacking faults is clearly governing the pinning performance.

In addition to the effect of the vortex pinning landscape, the superconducting properties of cuprates, strongly depend on the carrier concentration. In particular, the critical current density can be significantly enhanced by achieving the overdoped state due to an increase of the condensation energy [15, 28]. Figure 8 shows the average values of the self-field critical current density as a function of their carrier density, n_H, obtained for several pristine stoichiometric films grown at 810 °C (four samples) and Ba-deficient films grown at 810 °C (three samples) and 750 °C (four samples). The n_H value obtained for standard films grown at 810 °C with stoichiometric TFA solution with $J_c^{sf} \sim 4$–5 MA cm^{-2} is the one expected for optimally doped films $n_H \sim 8.10^{21}$ cm^{-3} [29]. For the films grown with Ba-deficient solution however, we observe that the values of n_H appear at the overdoped region. Films grown at 810 °C show similar J_c^{sf} values than those obtained for standard stoichiometric but slightly higher $n_H \sim 11.10^{21}$ cm^{-3}. Interestingly, Ba-deficient films grown at 750 °C show the highest charge carrier density with $n_H \sim 14 \times 10^{21}$ cm^{-3} and

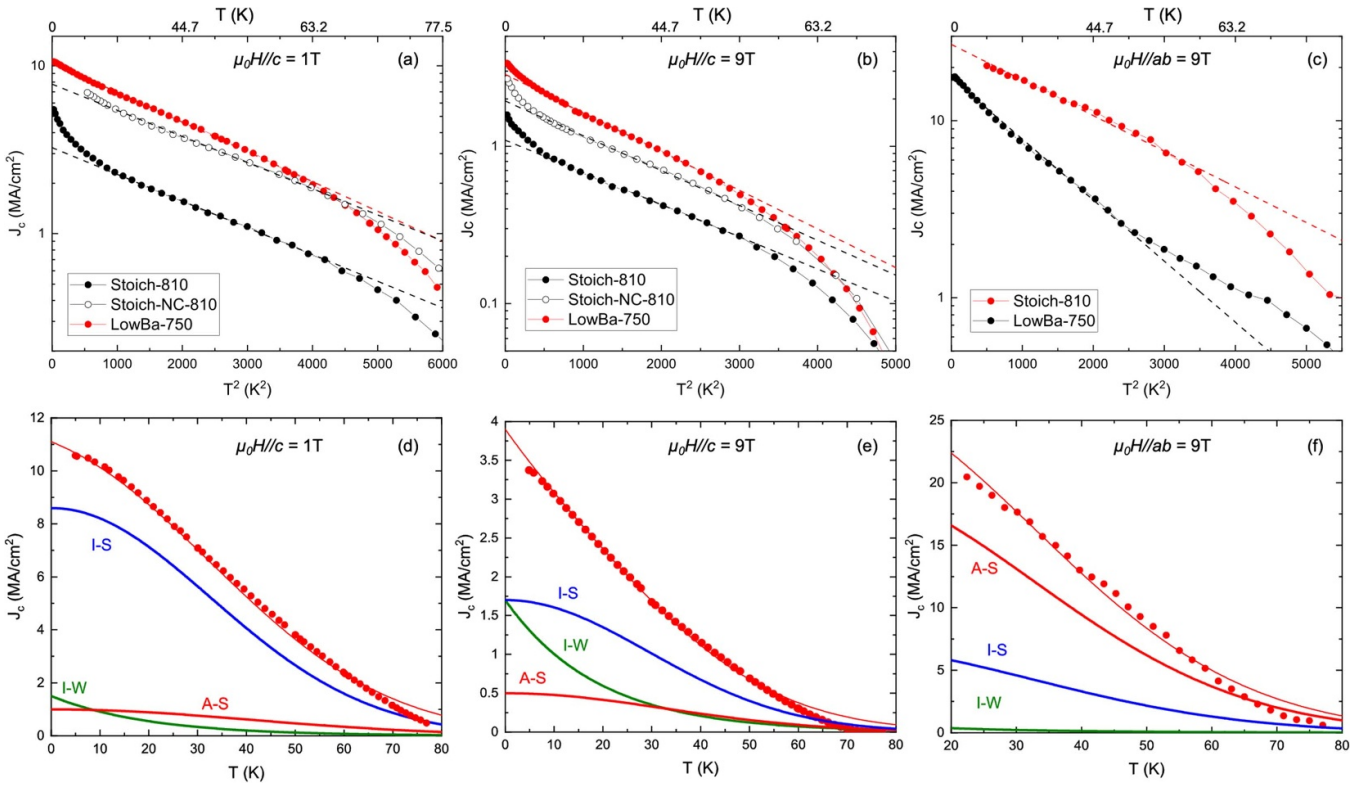

Figure 7. Log J_c versus T^2 at (a) 1 T, *H*//*c*, (b) 9 T, *H*//*c* and (c) 9 T, *H*//*ab*, measured for Stoich-810, Stoich-NC-810 and LowBa-750. (d), (e) and (f) show the temperature dependence of the weight of anisotropic-strong (A-S), isotropic-strong (I-S) and isotropic-weak (I-W) critical current density contributions for the LowBa-750 sample.

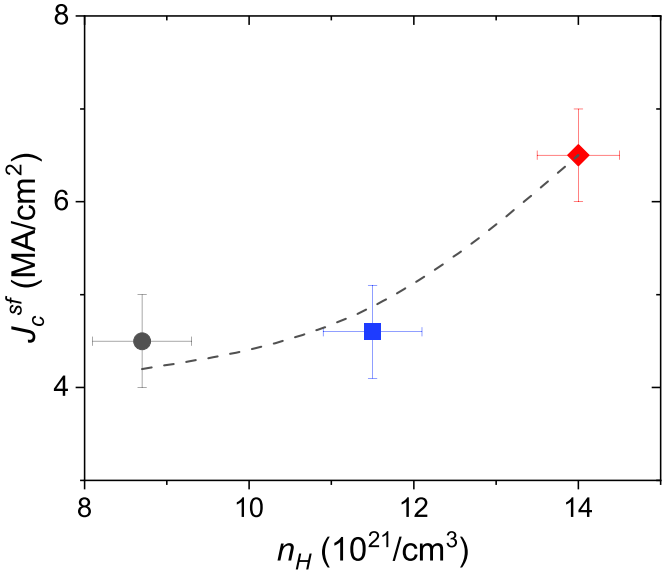

Figure 8. Self-field critical current density values at 77 K as a function the carrier density obtained at 300 K for pristine stoichiometric films (closed black dots), Ba-deficient films grown at 810 °C (closed blue squares) and Ba-deficient films grown at 750 °C (closed red diamonds).

large values of $J_c^{sf} \sim 6$–7 MA cm^{-2} can be obtained. The enhancement of the carrier density, and associated J_c^{sf}, can be correlated with a high density of stacking faults, suggesting that the induced disorder and nanostrain within the YBCO matrix may enhance the oxygen diffusion thus allowing to easily achieve an underdoped state.

4. Conclusions

The pinning performance of Ba-deficient samples grown at low temperature (750 °C) has been characterised through transport measurements and compared with a standard pristine film and a nancomposite with BHO nanoparticles grown at

higher temperature (810 °C). The results show that by reducing the growth temperature very high self-field critical current density values are obtained with smoth $J_c(H)$ dependences similar those obtained in nanocomposites. By measuring the temperature, field and angular dependence of J_c we have found that a highly effective pinning landscape is induced in the films grown at 750 °C mainly associated to the formation of a large number of stacking faults, observed by TEM images. Moreover, those films show very high values of J_c^{sf} which may be associated to a large carrier concentration at the overdoped state. Consequently, the use of Ba-deficient solutions showing a large *c*-axis epitaxial YBCO growth window appears as a very appealing way to tune both pinning landscape and the carrier density of YBCO pristine films and thus maximize their superconducting performance. It is worth pointing out that the addition of nanoparticles in the YBCO matrix not only generates pinning due to induced stacking faults and the associated strain but it is also possible to achieve a synergetic effect, with additional pinning coming from small nanoparticles [30, 31]. Thus, the combined effect of Ba-deficient precursor solution, low temperature growth and the addition of small nanoparticles may boost the pining performance of the films.

Data availability statement

All data that support the findings of this study are included within the article (and any supplementary files).

Acknowledgments

This work has been carried out within the framework of the EUROfusion Consortium and has received funding from the Euratom Research and Training Programme 2014–2018 and 2019–2020 under Grant Agreement No. 633 053. The views and opinions expressed herein do not necessarily reflect those of the European Commission. TEM analysis was funded from the EU Horizon 2020 research and innovation program under grant agreement 823717—ESTEEM3. The authors acknowledge financial support from Spanish Ministry of Economy and Competitiveness through the 'Severo Ochoa' Programme for Centres of Excellence in R&D (SEV-2015-0496 and CEX2019-000917-S), SuMaTe RTI2018-095853-B-C21, cofinanced by the European Regional Development Fund), the Catalan Government with Grant 2017-SGR-1519 and the EU COST action NANOCOHYBRI CA16218. We also acknowledge the Scientific Services at ICMAB. J A like to thank the UAB PhD program in Materials Science.

ORCID iDs

Jordi Alcalà https://orcid.org/0000-0001-5440-9061
Xavier Obradors https://orcid.org/0000-0003-4592-7718
Giuseppe Celentano https://orcid.org/0000-0001-6017-0739
Anna Palau https://orcid.org/0000-0002-2217-164X

References

[1] Mele P, Prassides K, Tarantini C, Palau A, Badica P, Jha A K and Endo T 2020 *Superconductiviy from Materials Science to Practical Applications* (Switzerland: Springer) (https://doi.org/10.1007/978-3-030-23303-7)
[2] Obradors X and Puig T 2014 Coated conductors for power applications: materials challenges *Supercond. Sci. Technol.* **27** 044003
[3] MacManus-Driscoll J L and Wimbush S C 2021 Processing and application of high-temperature superconducting coated conductors *Nat. Rev. Mater.* **6** 587–604
[4] Jha A K and Matsumoto K 2019 Superconductive REBCO thin films and their nanocomposites: the role of rare-earth oxides in promoting sustainable energy *Front. Phys.* **7** 82
[5] Palmer X *et al* 2016 Solution design for low-fluorine trifluoroacetate route to $YBa_2Cu_3O_7$ films *Supercond. Sci. Technol.* **29** 24002
[6] Li M, Cayado P, Erbe M, Jung A, Hanish J, Holzapfel B, Liu Z and Cai C 2020 Rapid pyrolysis of $SmBa_2Cu_3O_{7-\delta}$ films in CSD-MOD using extremely-low-fluorine solutions *Coatings* **10** 31
[7] Pinto V, Vannozzi A, Armenio A A, Rizzo F, Masi A, Santoni A, Meledin A, Ferrarese F M, Orlanducci S and Celentano G 2020 Chemical solution deposition of YBCO films with Gd excess *Coatings* **10** 1
[8] Ternero P *et al* 2021 Low-fluorine Ba-deficient solutions for high-performance superconducting YBCO films *Coatings* **11** 199
[9] Izumi T, Yoshizumi M, Miura M, Nakaoka N, Ichikawa Y, Sutoth Y, Miyata S, Fukushima H and Yamada Y S 2009 *Physica* C **469** 1322
[10] Teranishi R *et al* 2009 Crystal growth of Ba concentration controlled YBCO films by TFA-MOD process *IEEE Trans. Appl. Supercond.* **19** 3200
[11] Xie Z, Li Z, Lu H, Xu J, Luo X, Zhu Y and Wang Y 2020 Manipulation of $G1Ba_2Cu_3O_{7-x}$ Film properties by simply changing growth temperature with RF sputtering method *J. Phys.: Conf. Ser.* **1637** 012069
[12] Feldmann D M, Ugurlu O, Maiorov B, Stan L, Holesinger T G, Civale L, Foltyn S R and Jia Q X 2007 Influence of growth temperature on critical current and magnetic flux pinning structures in $YBa_2Cu_3O_{7-x}$ *Appl. Phys. Lett.* **91** 162501
[13] Obradors X, Puig T, Ricart S, Coll M, Gazquez J, Palau A and Granados X 2012 Growth, nanostructure and vortex pinning in superconducting $YBa_2Cu_3O_7$ thin films based on trifluoroacetate solutions *Supercond. Sci. Technol.* **25** 123001
[14] van der Pauw L J 1958 A method of measuring the resistivity and Hall coefficient on lamellae of arbitrary shape *Phil. Tech. Rev.* **20** 220–4
[15] Stangl A, Palau A, Deutscher G, Obradors X and Puig T 2021 Ultra-high critical current densities of superconducting $YBa_2Cu_3O_{7-\delta}$ thin films in the overdoped state *Sci. Rep.* **11** 8176
[16] Kovács A, Schierholz R and Tillmann K 2016 FEI Titan G2 80–200 crewley *J. Large-scale Res. Facil.* **2** A43
[17] Vallès F, Palau A, Abraimov D, Jaroszynski J, Constantinescu A-M, Mundet B, Obradors X, Larbalestier D and Puig T 2022 Optimizing vortex pinning in $YBa_2Cu_3O_{7-x}$ superconducting films up to high magnetic field *Commun. Mater.* **3** 45
[18] Palau A *et al* 2018 Disentangling vortex pinning landscape in chemical solution deposited superconducting $YBa_2Cu_3O_{7-x}$ films and nanocomposites *Supercond. Sci. Technol.* **31** 034004
[19] De Keukeleere K *et al* 2016 Superconducting $YBa_2Cu_3O_{7-\delta}$ nanocomposites using preformed ZrO_2 nanocrystals:

growth mechanisms and vortex pinning properties *Adv. Electron. Mater.* **2** 1600161
[20] Llordés A *et al* 2012 Nanoscale strain-induced pair suppression as a vortex-pinning mechanism in high-temperature superconductors *Nat. Mater.* **11** 329–36
[21] Civale L, Maiorov B, MacManus-Driscoll J L, Wang H, Holesinger T G, Foltyn S R, Serquis A and Arendt P N 2005 Identification of intrinsic ab-plane pinning in $YBa_2Cu_3O_7$ thin films and coated conductors *IEEE Trans. Appl. Supercond.* **15** 2808–11
[22] Foltyn S R, Wang H, Civale L, Jia Q X, Arendt P N, Maiorov B, Li Y, Maley M P and MacManus-Driscoll J L 2005 Overcoming the barrier to 1000 A/cm width superconducting coatings *Appl. Phys. Lett.* **87** 162505
[23] Blatter G, Feigel'man M V, Geshkenbeinn V B, Larkin A I and Vinokur V M 1994 Vortices in high-temperature superconductors *Rev. Mod. Phys.* **66** 1125
[24] Nelson D R and Vinokur V M 1993 Boson localization and correlated pinning of superconducting vortex arrays *Phys. Rev.* B **48** 13060
[25] Blatter G, Geshkenbein V B and Larkin A I 1992 Blatter-scaling.Pdf *Phys. Rev. Lett.* **68** 875
[26] Puig T, Gutiérrez J, Pomar A, Llordés A, Gázquez J, Ricart S, Sandiumenge F and Obradors X 2008 Vortex pinning in chemical solution nanostructured YBCO films *Supercond. Sci. Technol.* **21** 034008
[27] Gazquez J *et al* 2016 Emerging diluted ferromagnetism in high-Tc superconductors driven by point defect clusters *Adv. Sci.* **3** 1500295
[28] Strickland N M, Semwal A, Williams G V M, Verebelyi D T and Zhang W 2004 Optimizing the doping state of YBCO coated conductors *Supercond. Sci. Technol.* **17** S473–6
[29] Castro H and Deutscher G 2004 Anomalous Fermi liquid behavior of overdoped high-Tc superconductors *Phys. Rev.* B **70** 174511
[30] Li Z, Coll M, Mundet B, Chamorro N, Vallès F, Palau A, Gazquez J, Ricart S, Puig T and Obradors X 2019 Control of nanostructure and pinning properties in solution deposited $YBa_2Cu_3O_{7-x}$ nanocomposites with preformed perovskite nanoparticles *Sci. Rep.* **9** 1–14
[31] Miura M *et al* 2017 Tuning nanoparticle size for enhanced functionality in perovskite thin films deposited by metal organic deposition *NPG Asia Mater.* **9** 447